Diamagnetic Response of Potassium-Adsorbed Multilayer FeSe Film

Gang Yao,[1] Ming-Chao Duan,[1] Ningning Liu,[1] Yanfu Wu,[1] Dan-Dan Guan,[1,2] Shiyong Wang,[1,2] Hao Zheng,[1,2] Yao-Yi Li,[1,2] Canhua Liu,[1,2,3,*] and Jin-Feng Jia[1,2,3,†]

[1]*Key Laboratory of Artificial Structures and Quantum Control (Ministry of Education), Shenyang National Laboratory for Materials Science, School of Physics and Astronomy, Shanghai Jiao Tong University, 800 Dongchuan Road, Shanghai 200240, China*

[2]*Collaborative Innovation Center of Advanced Microstructures, Nanjing 210093, China*

[3]*Tsung-Dao Lee Institute, Shanghai 200240, China*

(Received 8 April 2019; revised manuscript received 23 July 2019; published 20 December 2019)

Intrigued by the discovery of high-temperature superconductivity in a single unit-cell layer of FeSe film on $SrTiO_3$, researchers recently found large superconductinglike energy gaps in K-adsorbed multilayer FeSe films by angle-resolved photoemission and scanning tunneling spectroscopy. However, the existence and nature of the high-temperature superconductivity inferred by the spectroscopic studies has not been investigated by measurements of zero resistance or the Meissner effect due to the fragility of K atoms in air. Using a self-developed multifunctional scanning tunneling microscope, we succeed in observing the diamagnetic response of K-adsorbed multilayer FeSe films, and thus find a dome-shaped relation between the critical temperature (T_c) and K coverage. Intriguingly, T_c exhibits an approximately linear dependence on the superfluid density in the whole K adsorbed region. Moreover, the quadratic low-temperature variation in the London penetration depth indicates a sign-reversal order parameter. These results provide compelling information towards further understanding of the high-temperature superconductivity in FeSe-derived superconductors.

DOI: 10.1103/PhysRevLett.123.257001

Carrier doping is an effective approach to the realization of high-temperature superconductivity in cuprates and iron pnictides, resulting in a dome-shaped relation between critical temperature (T_c) and doped carrier density [1,2]. Similarly, in the case of a single unit-cell (1UC) layer of FeSe film grown on a $SrTiO_3(100)$ substrate (STO), electron transfer from the STO substrate to the FeSe layer is believed to play an essential role in the emergence of a large superconducting energy gap (ranging from 10 to 22 meV [3–5]) and a high T_c value (ranging from 20 to 109 K in different studies [5–8]). For a multilayer FeSe film on STO, in contrast, no superconductinglike energy gap could be observed, indicating that the electron doping is very limited to the first FeSe layer in close proximity to the STO substrate. Alternatively, researchers found another strategy to enhance superconductivity in multilayer or bulk FeSe by depositing alkali-metal (K or Na) atoms on the surface [9–12]. Such a top-down electron doping at appropriate K coverage (K_c) results in a superconducting-like energy gap closing at a temperature as high as ~48 K [9,10]. However, the superconductivity in the K-adsorbed FeSe multilayers (K/FeSe) has not been verified yet via measurements of zero resistance or the Meissner effect, which requires *in situ* experimental techniques to overcome the problem from vulnerability of K adatoms to air.

Recently, heavy electron doping in FeSe thin flakes and multilayer films could also be achieved via ionic liquid gating [13–15] and molecule intercalation, i.e., $(Li_{1-x}Fe_x)$OHFeSe crystal [16,17], respectively, and thus realizes superconductivity with T_c's above 40 K. Although the $(Li_{1-x}Fe_x)$OHFeSe single crystal has a very similar Fermi surface topology as that of single-layer FeSe/STO and K/FeSe films, i.e., only one electron pocket at the M point of the Brillouin zone and no hole pocket at the Γ point revealed in ARPES studies [18,19], there is no universal understanding on paring symmetry of these superconducting FeSe layers in different doping forms. In previous studies using scanning tunneling microscopy or spectroscopy (STM/S), it was found that the single-layer FeSe/STO is a plain s-wave [20] or a d-wave superconductor [21], while the $(Li_{1-x}Fe_x)$HOFeSe single crystal may have an $s^{\pm}$ pairing symmetry [22]. In contrast, the nature of the superconductivity in K/FeSe films has not been well studied yet. Moreover, a dome-shaped relation between the energy gap and doping level has been discovered in K/FeSe films [9–11,23,24], while only discrete T_c values were found in FeSe thin flakes by continuously tuning carrier concentration with a solid ionic gating technique [25]. It is therefore very natural to raise questions whether a continuous dome-shaped phase diagram exists or not in a FeSe-derived superconductor.

Based on a commercial STM with a four-electrode piezo scanner tube, we developed a multifunctional STM (STM+) that enables *in situ* four-point-probe electrical

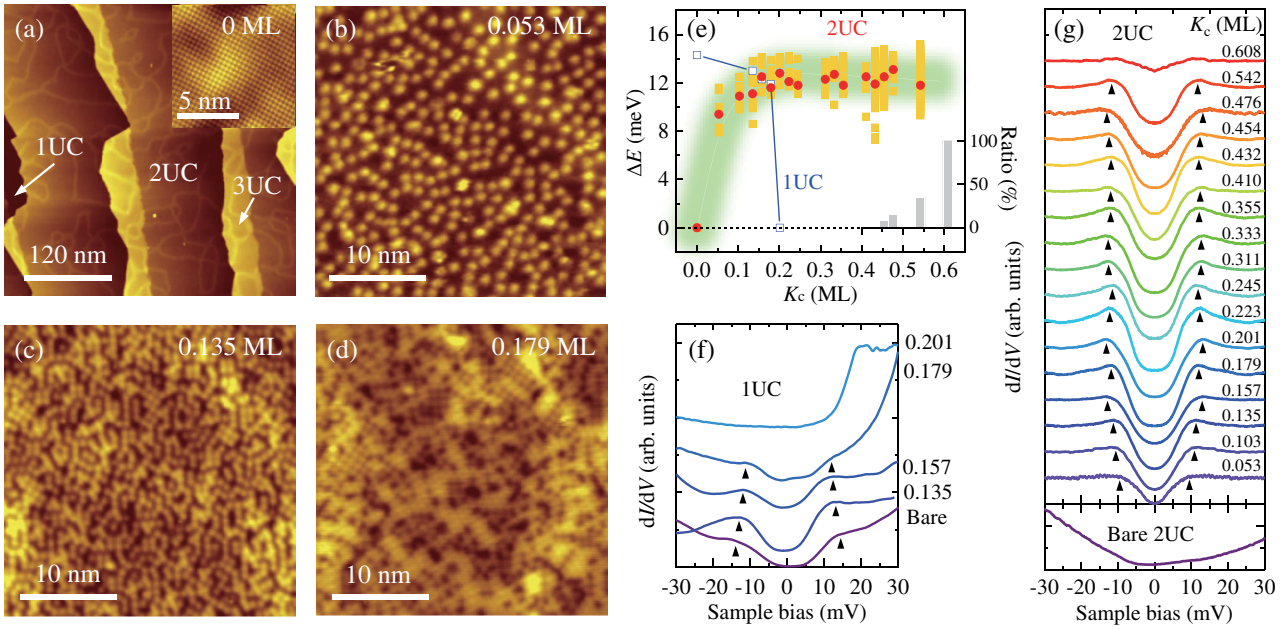

FIG. 1. STM/S characterization of K/FeSe thin film (sample No. 1; 2.3UC) taken at 7.8 K. (a) Large-scale STM image of the bare FeSe film. Inset: Atomic-resolution STM image acquired on a 2UC FeSe layer. (b)–(d) STM images acquired on 2UC FeSe layers at varied K_c indicated on each figure corner. Tunneling condition: $I_t = 100$ pA, (a) $V_s = 1.5$ V, inset: $V_s = 40$ mV; (b) $V_s = 1.0$ V; (c) $V_s = 1.3$ V; (d) $V_s = 1.0$ V. (e) Evolution of ΔE as a function of K_c on 1UC and 2UC FeSe layers. Each solid (open) square denotes the ΔE value deduced from individual dI/dV spectrum measured at an arbitrary position on 2UC (1UC) layers, while the solid circles represent the ΔE values of averaged spectra showing in (g). The embedded histogram represents the percentage of measured spectra showing no superconductinglike energy gap. (f) Typical dI/dV spectra at varied K_c on exposed 1UC FeSe layer. (g) Averaged dI/dV spectra at varied K_c on 2UC FeSe layer. Triangles in (f) and (g) denote the energy position of quasiparticle peaks.

measurement and two-coil mutual inductance measurement (TCMIM) in additional to general STM/S [26,27]. Using the STM+, we succeed in observing diamagnetic response of K/FeSe multilayers at various K_c, and thus reveal a continuous dome-shaped (T_c, K_c) phase diagram and experimental evidence for the macroscopic superconductivity in a K/FeSe film. Besides T_c, the information about the superconducting energy gap (ΔE), penetration depth (λ) and superfluid density (ρ_s) is also collected at various K_c's, from which spatial inhomogeneity of ΔE, quadratic low-temperature variation of λ and an approximate linear relation between T_c and ρ_s are revealed. These discoveries may be helpful for further understanding of superconductivity in FeSe-derived superconductors.

Detailed film growth and STM/S measurements are described in the Supplemental Material [28]. Figure 1(a) depicts the topographic image of a K/FeSe film with a nominal thickness of 2.3 UC (sample No. 1). The surface is mainly covered by 2UC FeSe layers with large atomically flat terraces, leaving small areas along step edges covered by patches of 1UC or 3UC layers, which is indicative of a step-flow growth mode. As K_c increases, K atoms are randomly and separately adsorbed on the FeSe surface at first [Fig. 1(b)], and then condense to form local 2×2 and $\sqrt{5} \times \sqrt{5}$ reconstructions at $K_c > 0.13$ monolayer (ML) [Figs. 1(c) and 1(d)]. Here 1 ML is defined as the areal density of the topmost Se sites, and K_c values are calibrated by counting K adatoms in STM images (see Fig. S2 [28]). Since these two reconstructions correspond to K_c's of 0.25 and 0.20 ML, respectively, it is naturally found that K adatoms start to pile up at $K_c \sim 0.22$ ML, where individual K adatoms cannot be recognized in some local areas appearing as bright clusters [Fig. 1(d)]. These STM observations are consistent with previous reports [11,29].

The exposed 1UC FeSe layer exhibits a superconducting energy gap, ΔE, with a value of 14.3 meV, which decreases gradually upon K adsorption at first and then dramatically drops to zero at $K_c \sim 0.20$ ML [Figs. 1(e) and 1(f)], consistent with previous studies [11,23]. Following previous reports [3,11,23,29], the gap value here is defined as the averaged energy position of the two quasiparticle peaks in dI/dV spectra (For the data analysis on ΔE, see the Supplemental Material [28]). In sharp contrast, 2UC FeSe layer shows a superconducting energy gap only after K adsorption, and the spatially averaged gap value increases with K_c and saturates at the optimal doping coverage, K_c ~0.22 ML [Figs. 1(e) and 1(g)]. It is found that the energy gap exhibits a spatial variation upon K adsorption, and the variation becomes more remarkable at higher K_c beyond 0.45 ML, from which spectra without energy gap (zero-gap spectra) start to emerge. The percentage of the zero-gap spectra increases with K_c and reaches 100% at ~0.61 ML,

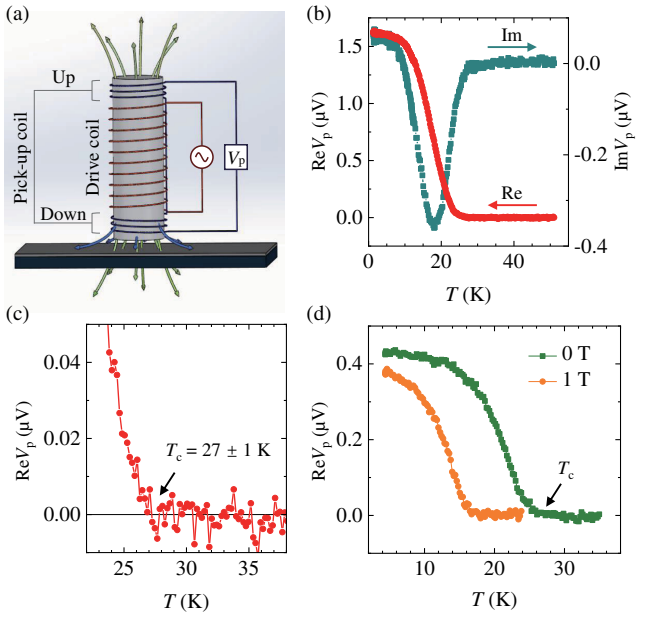

FIG. 2. A typical TCMIM result of K/FeSe film (sample No. 2; 2.5UC) at $K_c = 0.225$ ML. (a) Schematic illustration of the measurement setup. Green arrows denote the magnetic flux excited by the drive coil and blue arrows represent the magnetic flux screened by the superconducting sample. (b) Real and Imaginary parts of V_p measured as a function of temperature. The amplitude and frequency of I_{in} are 200 μA and 9991 Hz, respectively. (c) Zoom-in of the measured $\mathrm{Re}V_p$ curve showing the remarkable onset of superconducting transition at $T_c = 27$ K, as indicated by the arrow. (d) Comparison of $\mathrm{Re}V_p(T)$ curves measured with and without an external magnetic field of 1 T in the out-of-plane direction. Arrow indicates the position of T_c, which shifts from 27 to 17 K. The amplitude and frequency of I_{in} are 20 μA and 29 991 Hz, respectively.

as inset of Fig. 1(e) shows. A very similar electronic phase diagram was also obtained by analyzing the spectra with the BCS-Dynes theory [30] to extract the gap values (see Fig. S4 [28]).

The mutual inductance technique has been well used in studying diamagnetic response of various superconductors and in elucidating nature of superconductivity in previous studies [31–36]. The setup of the TCMIM system used here is schematically illustrated in Fig. 2(a). An alternating current I_{in} applied to the drive coil induces an alternating voltage V_p in the differential pick-up coil. Detailed measurements are referred to in the Supplemental Material [28]. Figure 2(b) exemplifies the temperature dependence of V_p measured on a K/FeSe film at $K_c = 0.225$ ML with a nominal FeSe thickness of 2.5 UC (sample No. 2). Clearly the real (imaginary) part of V_p, $\mathrm{Re}(V_p)$ [$\mathrm{Im}(V_p)$], starts to increase (decrease) at around 27 K when temperature decreases [see Fig. 2(c) for the determination of T_c]. This measurement result is a direct evidence for the diamagnetic response of the K-adsorbed FeSe films showing a superconducting transition, which has been only inferred in previous spectrosicopic studies [9–11,23,24,29]. The above conclusion on the superconducting transition is corrobarated by applying an external magnetic field of 1 T perpendicular to the sample surface, which remarkably reduces T_c, as shown in Fig. 2(d).

The effect of electron doping on the superconductivity in multilayer FeSe films is revealed by measuring a series of $\mathrm{Re}V_p(T)$ curves on sample No. 2 at varied K_c [Fig. 3(a)], from which a dome-shaped (T_c, K_c) phase diagram is obtained [Fig. 3(b)]. The STM observations reveal that the FeSe film consists of 71.6% of 2UC, 24.3% of 3UC, and 4.1% of 1UC layers (see Fig. S5). As the transition is observed at only one critical temperature in each $\mathrm{Re}V_p(T)$ curve but not at two, the transition signal should be dominated by 2UC layers and the superconductivity in 3UC layers does not manifest itself in the TCMIM results. Actually, as the typical width of 3UC layers is about 100 nm, much smaller than the in-plane penetration depth of FeSe (405 nm at zero temperature) [37], the additional supercurrent aroused by the superconducting transition of 3UC layers should make a negligible contribution to the $\mathrm{Re}V_p(T)$ intensity. Therefore, the dome-shaped phase diagram mainly reflects the intrinsic property of 2-UC FeSe layers. These results have been well reproduced in another K/FeSe thin film of sample No. 3, as shown in Fig. S6 [28]. It is noted that the continuous dome-shaped phase diagram revealed here is in sharp contrast to the discrete superconducting phase diagram reported very recently in a FeSe thin flake by tuning carrier concentration with a solid ionic gating technique [25].

The evolution of T_c as a function of K_c has a strong correlation with that of ΔE shown in Fig. 1(g), although they are taken from two FeSe film samples with a little different nominal thickness. Both T_c and ΔE increase remarkably with K_c till ~0.2 ML, which is the onset of the optimal doping coverage inferred in the (T_c, K_c) phase diagram. Beyond 0.2 ML, both T_c and ΔE vary little until 0.4 ML, above which zero-gap spectra emerge and ΔE values disperse more remarkably in STS measurements while T_c decreases evidently. The variation of ΔE and T_c with K_c indicates that electron doping increases the paring potential and enhances the superconductivity in the K/FeSe film at K_c below 0.4 ML. Above this K_c, the superconductivity is suppressed due to emergence of zero-gap regions that are probably resulted from a strong phase fluctuation. At $K_c > 0.6$ ML, the superconducting transition with $T_c \sim 5$ K revealed in $\mathrm{Re}V_p(T)$ curves could be attributed to the FeSe/STO interface since there was no superconductinglike dI/dV spectrum observed on the K-adsorbed FeSe film surface.

The T_c values found in the optimal doping region are 27–29 K, which is quite lower than that expected from previous ARPES studies having observed a gap closing at ~48 K [9,10]. It is noted that we have observed a superconducting transition with the highest T_c of 37.4 K in the

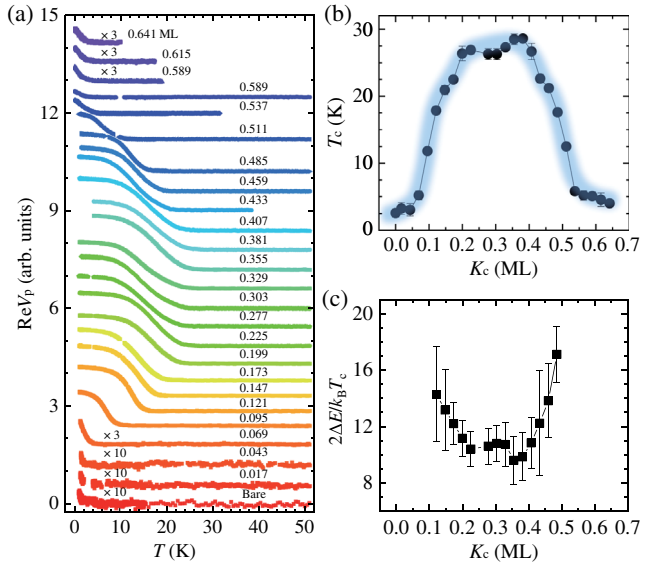

FIG. 3. TCMIM results of K/FeSe film (sample No. 2; 2.5UC) at varied K_c. (a) Temperature dependence of ReV_p measured on the sample film at varied K_c. (b) Evolution of T_c deduced from (a) as a function of K_c. The vertical error bars reflect the uncertainty in determining the T_c values, while the horizontal error bars on K_c are smaller than the size of the symbols. (c) K_c dependence of $2\Delta E/k_BT_c$. The error bars reflect the variation of gap values at each K_c.

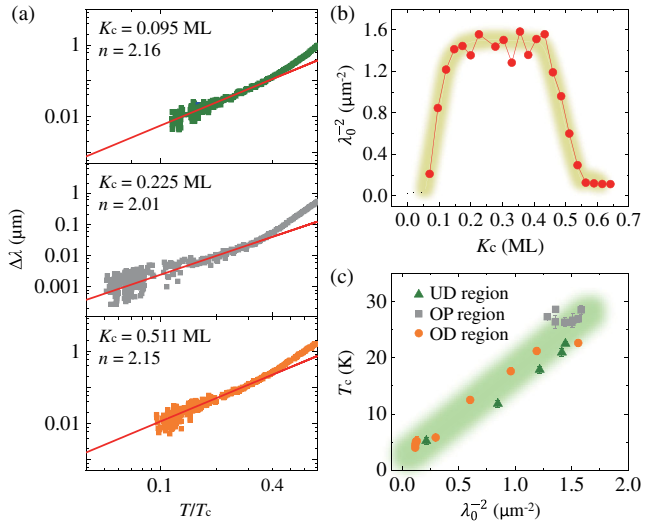

FIG. 4. London penetration depth and superfluid density deduced from the TCMIM results on sample No. 2. (a) Low-temperature variation of penetration depth obtained at three representative K_c. Solid lines are power-law fitting results within the low temperature region ($T < T_c/3$). (b) Evolution of the deduced superfluid density as a function of K_c. (c) Approximate linear relationship between T_c and superfluid density.

K/FeSe thin film of sample No. 1 at $K_c \sim 0.18$ ML, as shown in Fig. S7. Unfortunately, however, there are small half-UC $K_xFe_2Se_2$ islands come into form at $K_c \sim 0.22$ ML due to the unintentional sample's warming up during K adsorptions. The $K_xFe_2Se_2$ islands cover more and more surface areas with increasing K_c (Fig. S7), and thus make the sample No. 1 inappropriate for the following investigation. In contrast, a more careful sample cooling process was conducted during K adsorption for samples No. 2 and No. 3, and thus no half-UC $K_xFe_2Se_2$ island was observed on their surfaces (see Fig. S5 [28]), which makes the results quite reproducible.

Giving insight into the nature of superconductivity, the London penetration depth $\lambda(T)$ is calculated from $V_p(T)$ by following a widely used numerical analysis [38,39], in which the obtained λ value is overestimated but its ratio to the value at zero temperature λ_0, is accurate. Enumerated in Fig. 4(a) are three typical sets of $\lambda(T)$ calculated from the experimental data $V_p(T)$ taken at K_c in underdoped, optimal-doped, and overdoped regions, respectively. It is found that the low-temperature (empirically up to $T_c/3$) variations of $\Delta\lambda$ for all K_c's follow a power-law relation, $\Delta\lambda = \lambda(T) - \lambda_0 = \alpha T^n$, in which α is a meaningless scaling coefficient and the exponent n provides information about the symmetry of the underlying order parameter [40]. The power-law fitting gives n ranging from 2.01 to 2.16, very close to the value of 2, which indicates a sign-reversal order parameter previously revealed in many unconventional superconductors including d-wave cuprates in the presence of moderate scattering [41,42] and $s^{\pm}$-wave Fe-based superconductors at the dirty limit [43–45]. As no spectroscopic studies in STM or ARPES found any signature of d-wave superconductivity in K-adsorbed multilayer FeSe [9–11,24], the $s^{\pm}$ pairing symmetry seems to be more plausible for the interpretation of the behavior of $\lambda(T)$ discovered here. This idea is consistent with the conclusion of a recent STM/S work revealing the $s^{\pm}$ pairing symmetry in a Zn-doped $(Li_{1-x}Fe_x)$HOFeSe single crystal [22], which is another FeSe-derived superconductor without a hole pocket at the Γ point [18,19].

Figure 4(b) shows the variation of zero-temperature superfluid density, $\rho_{s0} \propto \lambda_0^{-2}$, as a function of K_c. It exhibits a dome shape very similar to that of the (T_c, K_c) phase diagram, resulting in an approximate linear dependence of T_c on ρ_{s0} in both underdoped and overdoped regions [Fig. 4(c)]. Such a linear relation between T_c and ρ_{s0} is known as Uemura's law [46], which has been found in many cuprate superconductors [47–49] and some Fe-based superconductors [16,50–52]. There are mainly two scenarios for the interpretation: one attributes to phase fluctuations that become more significant with lower superfluid density [53], and the other is the dirty BCS theory that supposes T_c be set primarily by the energy gap required to break a Cooper pair [54,55]. For an underdoped cuprate superconductor, the scenario of phase fluctuations is likely accepted since its ρ_{s0} is usually quite low. For an overdoped cuprate superconductor, however, it has remained the subject of intense debate [56–60], partly because disorder may directly influence T_c, ρ_{s0}, and Δ,

and thus complicate the causal relationships among these parameters.

In the present case of K/FeSe films, the variation of the three parameters with K_c has been all collected, from which we find the phase fluctuations may play an important role in the observed synchronized variation of T_c and ρ_{s0}, although the contribution of disorders could not be excluded completely. The gap ratio of $2\Delta E/k_B T_c$ is about 10 in the optimal-doping region and increases remarkably in both underdoped and overdoped regions, as shown in Fig. 3(c). It is noted that even lower gap values extracted from BCS fitting are used, the gap ratio is still more than 6 and not constant [see Fig. S4(d)]. The large values of the gap ratio imply a strong coupling and its non-constant evolution is also beyond the conventional BCS scenario.

In summary, we have unambiguously confirmed the emergence of superconductivity, and hence the dome-shaped phase diagram in K-adsorbed multilayer FeSe films with a self-developed STM+ containing an *in situ* TCMIM system. The T^2 dependence of penetration depth at low temperature implies a sign-reversal pairing symmetry in the K/FeSe film, and the synchronized variation of T_c and ρ_{s0} implies that the transition temperature should be determined by phase stiffness rather than pairing potential. This is consistent with the experimental result that the ratio of $2\Delta E/k_B T_c$ is not constant.

This work was financially supported by the National Basic Research Program of China (Grants No. 2016YFA0300403, No. 2016YFA0301003), NSFC (Grants No. 11574202, No. 11874256, No. 11521404, No. 11874258, No. 11634009, No. U1632102, No. 11861161003, No. 11674222, No. 11790313, and No. 11674226), the Key Research Program of CAS (Grant No. XDPB08-2), and the Strategic Priority Research Program of CAS (Grant No. XDB28000000). C. L. and J. F. J. acknowledge additional support from a Shanghai talent program.

G. Y. and M. C. D. contributed equally to this work.

*To whom all correspondence should be addressed.
canhualiu@sjtu.edu.cn
†To whom all correspondence should be addressed.
jfjia@sjtu.edu.cn

[1] P. A. Lee, N. Nagaosa, and X. G. Wen, Doping a Mott insulator: Physics of high-temperature superconductivity, Rev. Mod. Phys. **78**, 17 (2006).

[2] G. R. Stewart, Superconductivity in iron compounds, Rev. Mod. Phys. **83**, 1589 (2011).

[3] Q. Y. Wang, Z. Li, W. H. Zhang, Z. C. Zhang, J. S. Zhang, W. Li, H. Ding, Y. B. Ou, P. Deng, K. Chang, J. Wen, C. L. Song, K. He, J. F. Jia, S. H. Ji, Y. Y. Wang, L. L. Wang, X. Chen, X. C. Ma, and Q. K. Xue, Interface-induced high-temperature superconductivity in single unit-cell FeSe films on $SrTiO_3$, Chin. Phys. Lett. **29**, 037402 (2012).

[4] S. He *et al.*, Phase diagram and electronic indication of high-temperature superconductivity at 65 K in single-layer FeSe films, Nat. Mater. **12**, 605 (2013).

[5] D. F. Liu *et al.*, Electronic origin of high-temperature superconductivity in single-layer FeSe superconductor, Nat. Commun. **3**, 931 (2012).

[6] L. Z. Deng, B. Lv, Z. Wu, Y. Y. Xue, W. H. Zhang, F. S. Li, L. L. Wang, X. C. Ma, Q. K. Xue, and C. W. Chu, Meissner and mesoscopic superconducting states in 1–4 unit-cell FeSe films, Phys. Rev. B **90**, 214513 (2014).

[7] J. F. Ge, Z. L. Liu, C. Liu, C. L. Gao, D. Qian, Q. K. Xue, Y. Liu, and J. F. Jia, Superconductivity above 100 K in single-layer FeSe films on doped $SrTiO_3$, Nat. Mater. **14**, 285 (2015).

[8] Z. C. Zhang, Y. H. Wang, Q. Song, C. Liu, R. Peng, K. A. Moler, D. L. Feng, and Y. Y. Wang, Onset of the Meissner effect at 65 K in FeSe thin film grown on Nb-doped $SrTiO_3$ substrate, Sci. Bull. **60**, 1301 (2015).

[9] Y. Miyata, K. Nakayama, K. Sugawara, T. Sato, and T. Takahashi, High-temperature superconductivity in potassium-coated multilayer FeSe thin films, Nat. Mater. **14**, 775 (2015).

[10] C. H. P. Wen, H. C. Xu, C. Chen, Z. C. Huang, X. Lou, Y. J. Pu, Q. Song, B. P. Xie, M. Abdel-Hafiez, D. A. Chareev, A. N. Vasiliev, R. Peng, and D. L. Feng, Anomalous correlation effects and unique phase diagram of electron-doped FeSe revealed by photoemission spectroscopy, Nat. Commun. **7**, 10840 (2016).

[11] C. Tang, D. Zhang, Y. Zang, C. Liu, G. Zhou, Z. Li, C. Zheng, X. Hu, C. Song, S. Ji, K. He, X. Chen, L. Wang, X. Ma, and Q. K. Xue, Superconductivity dichotomy in K-coated single and double unit cell FeSe films on $SrTiO_3$, Phys. Rev. B **92**, 180507(R) (2015).

[12] J. J. Seo, B. Y. Kim, B. S. Kim, J. K. Jeong, J. M. Ok, J. S. Kim, J. D. Denlinger, S. K. Mo, C. Kim, and Y. K. Kim, Superconductivity below 20 K in heavily electron-doped surface layer of FeSe bulk crystal, Nat. Commun. **7**, 11116 (2016).

[13] B. Lei, J. H. Cui, Z. J. Xiang, C. Shang, N. Z. Wang, G. J. Ye, X. G. Luo, T. Wu, Z. Sun, and X. H. Chen, Evolution of High-Temperature Superconductivity from a Low-T_c Phase Tuned by Carrier Concentration in FeSe Thin Flakes, Phys. Rev. Lett. **116**, 077002 (2016).

[14] K. Hanzawa, H. Sato, H. Hiramatsu, T. Kamiya, and H. Hosono, Electric field-induced superconducting transition of insulating FeSe thin film at 35 K, Proc. Natl. Acad. Sci. U.S.A. **113**, 3986 (2016).

[15] J. Shiogai, Y. Ito, T. Mitsuhashi, T. Nojima, and A. Tsukazaki, Electric-field-induced superconductivity in electrochemically etched ultrathin FeSe films on $SrTiO_3$ and MgO, Nat. Phys. **12**, 42 (2016).

[16] M. Burrard-Lucas, D. G. Free, S. J. Sedlmaier, J. D. Wright, S. J. Cassidy, Y. Hara, A. J. Corkett, T. Lancaster, P. J. Baker, S. J. Blundell, and S. J. Clarke, Enhancement of the superconducting transition temperature of FeSe by intercalation of a molecular spacer layer, Nat. Mater. **12**, 15 (2013).

[17] X. F. Lu, N. Z. Wang, H. Wu, Y. P. Wu, D. Zhao, X. Z. Zeng, X. G. Luo, T. Wu, W. Bao, G. H. Zhang, F. Q. Huang, Q. Z. Huang, and X. H. Chen, Coexistence of

superconductivity and antiferromagnetism in $(Li_{0.8}Fe_{0.2})$OHFeSe, Nat. Mater. **14**, 325 (2015).

[18] L. Zhao *et al.*, Common electronic origin of superconductivity in (Li,Fe)OHFeSe bulk superconductor and single-layer FeSe/$SrTiO_3$ films, Nat. Commun. **7**, 10608 (2016).

[19] X. H. Niu, R. Peng, H. C. Xu, Y. J. Yan, J. Jiang, D. F. Xu, T. L. Yu, Q. Song, Z. C. Huang, Y. X. Wang, B. P. Xie, X. F. Lu, N. Z. Wang, X. H. Chen, Z. Sun, and D. L. Feng, Surface electronic structure and isotropic superconducting gap in $(Li_{0.8}Fe_{0.2})$OHFeSe, Phys. Rev. B **92**, 060504(R) (2015).

[20] Q. Fan, W. H. Zhang, X. Liu, Y. J. Fan, M. Q. Ren, R. Peng, H. C. Xu, B. P. Xie, J. P. Hu, T. Zhang, and D. L. Feng, Plain *s*-wave superconductivity in single-layer FeSe on $SrTiO_3$ probed by scanning tunnelling microscopy, Nat. Phys. **11**, 946 (2015).

[21] Z. Ge, C. Yan, H. Zhang, D. Agterberg, M. Weinert, and L. Li, Evidence for *d*-wave superconductivity in single layer FeSe/$SrTiO_3$ probed by quasiparticle scattering off step edges, Nano Lett. **19**, 2497 (2019).

[22] Z. Du, X. Yang, D. Altenfeld, Q. Gu, H. Yang, I. Eremin, P. J. Hirschfeld, I. I. Mazin, H. Lin, X. Zhu, and H. H. Wen, Sign reversal of the order parameter in $(Li_1 - {}_xFe_x)$ $OHFe_{1-y}Zn_ySe$, Nat. Phys. **14**, 134 (2018).

[23] W. H. Zhang, X. Liu, C. H. Wen, R. Peng, S. Y. Tan, B. P. Xie, T. Zhang, and D. L. Feng, Effects of surface electron doping and substrate on the superconductivity of epitaxial FeSe films, Nano Lett. **16**, 1969 (2016).

[24] C. L. Song, H. M. Zhang, Y. Zhong, X. P. Hu, S. H. Ji, L. L. Wang, K. He, X. C. Ma, and Q. K. Xue, Observation of Double-Dome Superconductivity in Potassium-Doped FeSe Thin Films, Phys. Rev. Lett. **116**, 157001 (2016).

[25] T. P. Ying, M. X. Wang, X. X. Wu, Z. Y. Zhao, Z. Z. Zhang, B. Q. Song, Y. C. Li, B. Lei, Q. Li, Y. Yu, E. J. Cheng, Z. H. An, Y. Zhang, X. Y. Jia, W. Yang, X. H. Chen, and S. Y. Li, Discrete Superconducting Phases in FeSe-Derived Superconductors, Phys. Rev. Lett. **121**, 207003 (2018).

[26] J. F. Ge, Z. L. Liu, C. L. Gao, D. Qian, C. Liu, and J. F. Jia, Development of micro-four-point probe in a scanning tunneling microscope for *in situ* electrical transport measurement, Rev. Sci. Instrum. **86**, 053903 (2015).

[27] M. C. Duan, Z. L. Liu, J. F. Ge, Z. J. Tang, G.-Y. Wang, Z.-X. Wang, D. Guan, Y.-Y. Li, D. Qian, C. Liu, and J. F. Jia, Development of *in situ* two-coil mutual inductance technique in a multifunctional scanning tunneling microscope, Rev. Sci. Instrum. **88**, 073902 (2017).

[28] See Supplemental Material at http://link.aps.org/supplemental/10.1103/PhysRevLett.123.257001 for details of experimental methods and data analysis.

[29] C. J. Tang, C. Liu, G. Y. Zhou, F. S. Li, H. Ding, Z. Li, D. Zhang, Z. Li, C. L. Song, S. H. Ji, K. He, L. L. Wang, X. C. Ma, and Q. K. Xue, Interface-enhanced electron-phonon coupling and high-temperature superconductivity in potassium-coated ultrathin FeSe films on $SrTiO_3$, Phys. Rev. B **93**, 020507(R) (2016).

[30] R. C. Dynes, V. Narayanamurti, and J. P. Garno, Direct Measurement of Quasiparticle-Lifetime Broadening in a Strong-Coupled Superconductor, Phys. Rev. Lett. **41**, 1509 (1978).

[31] R. A. Doyle, D. Liney, W. S. Seow, A. M. Campbell, and K. Kadowaki, First-Order Decoupling Transition in the Vortex Lattice of $Bi_2Sr_2CaCu_2O_8$ from Local Mutual Inductance Measurements, Phys. Rev. Lett. **75**, 4520 (1995).

[32] A. Kamlapure, M. Mondal, M. Chand, A. Mishra, J. Jesudasan, V. Bagwe, L. Benfatto, V. Tripathi, and P. Raychaudhuri, Measurement of magnetic penetration depth and superconducting energy gap in very thin epitaxial NbN films, Appl. Phys. Lett. **96**, 072509 (2010).

[33] X. He, A. Gozar, R. Sundling, and I. Božović, High-precision measurement of magnetic penetration depth in superconducting films, Rev. Sci. Instrum. **87**, 113903 (2016).

[34] H. Nam, P. H. Su, and C. K. Shih, *In situ*/non-contact superfluid density measurement apparatus, Rev. Sci. Instrum. **89**, 043901 (2018).

[35] H. Nam, H. Chen, P. W. Adams, S. Y. Guan, T. M. Chuang, C. S. Chang, A. H. MacDonald, and C. K. Shih, Geometric quenching of orbital pair breaking in a single crystalline superconducting nanomesh network, Nat. Commun. **9**, 5431 (2018).

[36] Y. Wu, M. C. Duan, N. Liu, G. Yao, D. Guan, S. Wang, Y. Y. Li, H. Zheng, C. Liu, and J. F. Jia, Diamagnetic response of a superconducting surface superstructure: $Si(111) - \sqrt{7} \times \sqrt{3}$-In, Phys. Rev. B **99**, 140506(R) (2019).

[37] R. Khasanov, K. Conder, E. Pomjakushina, A. Amato, C. Baines, Z. Bukowski, J. Karpinski, S. Katrych, H. H. Klauss, H. Luetkens, A. Shengelaya, and N. D. Zhigadlo, Evidence of nodeless superconductivity in $FeSe_{0.85}$ from a muon-spin-rotation study of the in-plane magnetic penetration depth, Phys. Rev. B **78**, 220510(R) (2008).

[38] J. R. Clem and M. W. Coffey, Vortex dynamics in a type-II superconducting film and complex linear-response functions, Phys. Rev. B **46**, 14662 (1992).

[39] S. J. Turneaure, E. R. Ulm, and T. R. Lemberger, Numerical modeling of a two-coil apparatus for measuring the magnetic penetration depth in superconducting films and arrays, J. Appl. Phys. **79**, 4221 (1996).

[40] R. Prozorov and V. G. Kogan, London penetration depth in iron-based superconductors, Rep. Prog. Phys. **74**, 124505 (2011).

[41] P. J. Hirschfeld and N. Goldenfeld, Effect of strong scattering on the low-temperature penetration depth of a *d*-wave superconductor, Phys. Rev. B **48**, 4219 (1993).

[42] V. G. Kogan, R. Prozorov, and V. Mishra, London penetration depth and pair breaking, Phys. Rev. B **88**, 224508 (2013).

[43] V. Mishra, G. R. Boyd, S. Graser, T. Maier, P. J. Hirschfeld, and D. J. Scalapino, Lifting of nodes by disorder in extended-*s*-state superconductors: Application to ferropnictides, Phys. Rev. B **79**, 094512 (2009).

[44] C. Martin, M. E. Tillman, H. Kim, M. A. Tanatar, S. K. Kim, A. Kreyssig, R. T. Gordon, M. D. Vannette, S. Nandi, V. G. Kogan, S. L. Bud'ko, P. C. Canfield, A. I. Goldman, and R. Prozorov, Nonexponential London Penetration Depth of FeAs-Based Superconducting RFeAs$O_{0.9}F_{0.1}$ (R = La, Nd) Single Crystals, Phys. Rev. Lett. **102**, 247002 (2009).

[45] K. Cho, A. Fente, S. Teknowijoyo, M. A. Tanatar, K. R. Joshi, N. M. Nusran, T. Kong, W. R. Meier, U. Kaluarachchi, I. Guillamón, H. Suderow, S. L. Bud'ko, P. C. Canfield, and

R. Prozorov, Nodeless multiband superconductivity in stoichiometric single-crystalline $CaKFe_4As_4$, Phys. Rev. B **95**, 100502(R) (2017).

[46] Y. J. Uemura *et al.*, Universal Correlations between T_c and n_s/m^* (Carrier Density over Effective Mass) in High-T_c Cuprate Superconductors, Phys. Rev. Lett. **62**, 2317 (1989).

[47] Y. Uemura, L. Le, G. Luke, B. Sternlieb, W. Wu, J. Brewer, T. Riseman, C. Seaman, M. Maple, M. Ishikawa, D. G. Hinks, J. D. Jorgensen, G. Saito, and H. Yamochi, Basic Similarities Among Cuprate, Bismuthate, Organic, Chevrel-Phase, and Heavy-Fermion Superconductors Shown by Penetration-Depth Measurements, Phys. Rev. Lett. **66**, 2665 (1991).

[48] I. Božović, X. He, J. Wu, and A. T. Bollinger, Dependence of the critical temperature in overdoped copper oxides on superfluid density, Nature (London) **536**, 309 (2016).

[49] I. Hetel, T. R. Lemberger, and M. Randeria, Quantum critical behaviour in the superfluid density of strongly underdoped ultrathin copper oxide films, Nat. Phys. **3**, 700 (2007).

[50] Z. Shermadini, H. Luetkens, A. Maisuradze, R. Khasanov, Z. Bukowski, H. H. Klauss, and A. Amato, Superfluid density and superconducting gaps of $RbFe_2As_2$ as a function of hydrostatic pressure, Phys. Rev. B **86**, 174516 (2012).

[51] L. Luan, T. M. Lippman, C. W. Hicks, J. A. Bert, O. M. Auslaender, J. H. Chu, J. G. Analytis, I. R. Fisher, and K. A. Moler, Local Measurement of the Superfluid Density in the Pnictide Superconductor $Ba(Fe_{1-x}Co_x)_2As_2$ across the Superconducting Dome, Phys. Rev. Lett. **106**, 067001 (2011).

[52] R. Khasanov, M. Bendele, A. Amato, K. Conder, H. Keller, H. H. Klauss, H. Luetkens, and E. Pomjakushina, Evolution of Two-Gap Behavior of the Superconductor $FeSe_{1-x}$, Phys. Rev. Lett. **104**, 087004 (2010).

[53] V. J. Emery and S. A. Kivelson, Importance of phase fluctuations in superconductors with small superfluid density, Nature (London) **374**, 434 (1995).

[54] N. R. Lee-Hone, J. S. Dodge, and D. M. Broun, Disorder and superfluid density in overdoped cuprate superconductors, Phys. Rev. B **96**, 024501 (2017).

[55] N. R. Lee-Hone, V. Mishra, D. M. Broun, and P. J. Hirschfeld, Optical conductivity of overdoped cuprate superconductors: Application to $La_{2-x}Sr_xCuO_4$, Phys. Rev. B **98**, 054506 (2018).

[56] N. R. Lee-Hone, H. U. Özdemir, V. Mishra, D. M. Broun, and P. J. Hirschfeld, From Mott to not: phenomenology of overdoped cuprates, arXiv:1902.08286.

[57] F. F. Tafti, F. Laliberté, M. Dion, J. Gaudet, P. Fournier, and L. Taillefer, Nernst effect in the electron-doped cuprate superconductor $Pr_{2-x}Ce_xCuO_4$: Superconducting fluctuations, upper critical field H_{c2}, and the origin of the T_c dome, Phys. Rev. B **90**, 024519 (2014).

[58] C. Collignon, B. Fauqué, A. Cavanna, U. Gennser, D. Mailly, and K. Behnia, Superfluid density and carrier concentration across a superconducting dome: The case of strontium titanate, Phys. Rev. B **96**, 224506 (2017).

[59] M. Thiemann, M. H. Beutel, M. Dressel, N. R. Lee-Hone, D. M. Broun, E. Fillis-Tsirakis, H. Boschker, J. Mannhart, and M. Scheffler, Single-Gap Superconductivity and Dome of Superfluid Density in Nb-Doped $SrTiO_3$, Phys. Rev. Lett. **120**, 237002 (2018).

[60] F. Mahmood, X. He, I. Božović, and N. P. Armitage, Locating the Missing Superconducting Electrons in the Overdoped Cuprates $La_{2-x}Sr_xCuO_4$, Phys. Rev. Lett. **122**, 027003 (2019).